Published OnlineFirst June 23, 2009; DOI: 10.1158/0008-5472.CAN-08-4410
Published Online First on June 23, 2009 as 10.1158/0008-5472.CAN-08-4410

Targeted *In vivo* Imaging of Integrin $\alpha_v\beta_6$ with an Improved Radiotracer and Its Relevance in a Pancreatic Tumor Model

Sven H. Hausner,[1] Craig K. Abbey,[3] Richard J. Bold,[4] M. Karen Gagnon,[1] Jan Marik,[1] John F. Marshall,[5] Cathy E. Stanecki,[1] and Julie L. Sutcliffe[1,2]

[1]Department of Biomedical Engineering and [2]Center for Molecular and Genomic Imaging, University of California Davis, Davis, California; [3]Department of Psychology, University of California Santa Barbara, Santa Barbara, California; [4]Division of Surgical Oncology, University of California Davis Medical Center, Sacramento, California; and [5]Tumour Biology Centre, Barts and The London Medical School, London, United Kingdom

Abstract

The cell surface receptor $\alpha_v\beta_6$ is epithelial specific, and its expression is tightly regulated; it is low or undetectable in adult tissues but has been shown to be increased in many different cancers, including pancreatic, cervical, lung, and colon cancers. Studies have described $\alpha_v\beta_6$ as a prognostic biomarker linked to poor survival. We have recently shown the feasibility of imaging $\alpha_v\beta_6$ *in vivo* by positron emission tomography (PET) using the peptide [^{18}F]FBA-A20FMDV2. Here, we describe improved $\alpha_v\beta_6$ imaging agents and test their efficacy in a mouse model with endogenous $\alpha_v\beta_6$ expression. The modified compounds maintained high affinity for $\alpha_v\beta_6$ and >1,000-fold selectivity over related integrins (by ELISA) and showed significantly improved $\alpha_v\beta_6$-dependent binding in cell-based assays (>60% binding versus <10% for [^{18}F]FBA-A20FMDV2). *In vivo* studies using either a melanoma cell line (transduced $\alpha_v\beta_6$ expression) or the BxPC-3 human pancreatic carcinoma cell line (endogenous $\alpha_v\beta_6$ expression) revealed that the modified compounds showed significantly improved tumor retention. This, along with good clearance of nonspecifically bound activity, particularly for the new radiotracer [^{18}F]FBA-PEG$_{28}$-A20FMDV2, resulted in improved PET imaging. Tumor/pancreas and tumor/blood biodistribution ratios of >23:1 and >47:1, respectively, were achieved at 4 hours. Significantly, [^{18}F]FBA-PEG$_{28}$-A20FMDV2 was superior to 2-[^{18}F]fluoro-2-deoxy-D-glucose ([^{18}F]FDG) in imaging the BxPC-3 tumors. Pancreatic ductal adenocarcinoma is highly metastatic and current preoperative evaluation of resectability using noninvasive imaging has limited success, with most patients having metastases at time of surgery. The fact that these tumors express $\alpha_v\beta_6$ suggests that this probe has significant potential for the *in vivo* detection of this malignancy, thus having important implications for patient care and therapy. [Cancer Res 2009;69(14):OF1–7]

Introduction

In recent years, positron emission tomography (PET) imaging, using 2-[^{18}F]fluoro-2-deoxy-D-glucose ([^{18}F]FDG), has become routine for detection of tumors and monitoring of treatment response (1–3). [^{18}F]FDG, a radiolabeled analogue of glucose, is taken up and trapped primarily in cells with high metabolism. As glucose hypermetabolism is commonly found in inflammation, as well as in many malignancies, distinguishing cancer from other hypermetabolic states remains a challenge (1, 4, 5). Although PET has been combined with other imaging modalities, most notably computed tomography (CT), which relies on subtle differences in soft tissue density to distinguish between normal and malignant tissues (5–7), [^{18}F]FDG-PET/CT still leaves considerable room for improvement in diagnosis and clinical management of many cancers (8). The availability of more disease-specific imaging agents (7) could help to mitigate the limited specificity of [^{18}F]FDG for malignant tissue. Rather than relying on slight changes in tissue density or metabolic rate alone, targeting disease-specific tissue markers could considerably aid in tumor detection and localization. The feasibility of this approach has been shown with [^{18}F]galacto-RGD, a small radiolabeled peptide used for PET imaging of the cancer-related integrin $\alpha_v\beta_3$ (9). In contrast to $\alpha_v\beta_3$, other members of the integrin family have received relatively little attention. However, newly emerging evidence indicates that $\alpha_v\beta_6$ may also be an important target for diagnosis and treatment of cancer (10–14). The integrin $\alpha_v\beta_6$ was first identified in a human pancreatic carcinoma cell line (15). Subsequent studies established that although $\alpha_v\beta_6$ is epithelial specific, its expression is low or undetectable in healthy adult tissues. Up-regulation has been recognized during tissue remodeling, including inflammation and wound healing (16–18). Significantly, expression has also been shown to be increased in many different cancers (13, 19). Among gastroenteropancreatic adenocarcinomas, $\alpha_v\beta_6$ expression was found to be strongest in pancreatic ductal adenocarcinomas (PDAC; ref. 20). Moreover, $\alpha_v\beta_6$ has recently been described as a prognostic indicator, with high levels of expression correlating with poor prognosis for cancer of the colon, cervix, lung, and stomach (10–12, 21). Antibody-blockade of $\alpha_v\beta_6$ was shown to inhibit tumor progression *in vivo* in animal models (13). Thus, mounting evidence implicates $\alpha_v\beta_6$ as an important and biologically relevant target for molecular imaging of cancer.

Recently, we showed the ability to selectively image $\alpha_v\beta_6$-expressing tumors *in vivo* with microPET using the $\alpha_v\beta_6$-specific [^{18}F]fluorobenzoyl-labeled peptide [^{18}F]FBA-A20FMDV2 (22). Whereas targeted imaging was achieved, low uptake and poor retention in the target tissue limited its general utility. For this current study, we conjugated small, monodisperse polyethylene glycol (PEG) polymers to A20FMDV2 to improve pharmacokinetics, generating the two new radiotracers [^{18}F]FBA-PEG$_{28}$-A20FMDV2 and [^{18}F]FBA-(PEG$_{28}$)$_2$-A20FMDV2. We report that both PEGylated A20FMDV2 variants showed significantly improved retention in two different $\alpha_v\beta_6$-expressing human tumor xenograft models: DX3puroβ6, a human melanoma cell line transduced to express $\alpha_v\beta_6$, and BxPC-3, a human pancreatic carcinoma cell line that endogenously expresses $\alpha_v\beta_6$. In the BxPC-3 model, retention of [^{18}F]FBA-PEG$_{28}$-A20FMDV2 in tumors was 12-fold greater than

Note: Supplementary data for this article are available at Cancer Research Online (http://cancerres.aacrjournals.org/).

Requests for reprints: Julie L. Sutcliffe, Department of Biomedical Engineering, Genomics and Biomedical, Sciences Facility, 451 Health Sciences Drive, University of California Davis, Davis, CA 95616. Phone: 530-754-7107; Fax: 530-754-5739; E-mail: jlsutcliffe@ucdavis.edu.

doi:10.1158/0008-5472.CAN-08-4410

Published OnlineFirst June 23, 2009; DOI: 10.1158/0008-5472.CAN-08-4410

retention of the non-PEGylated [^{18}F]FBA-A20FMDV2. Tumor/pancreas and tumor/blood ratios of >23:1 and >47:1, respectively, were achieved with [^{18}F]FBA-PEG$_{28}$-A20FMDV2 at 4 hours. The ability to noninvasively detect regional tumor invasion or occult metastatic disease using $\alpha_v\beta_6$ PET imaging would have a large effect on patient management, reducing the number of unnecessary surgeries of unresectable disease (23).

Materials and Methods

Reagents and cell lines. Reagents, materials, and DX3puro/DX3puroβ6 cell lines have been described previously (22). Pancreatic cancer cell lines were obtained from American Type Culture Collection. Transforming growth factor β1 human latency-associated peptide (TGFβ1–LAP) was purchased from Sigma. A Leica CM1850 cryostat (Leica Microsystems) was used for tissue sectioning.

Competitive binding ELISA. The *in vitro* efficacies of the peptides toward integrins $\alpha_v\beta_6$, $\alpha_v\beta_3$, $\alpha_v\beta_5$, $\alpha_5\beta_1$, and $\alpha_{IIb}\beta_3$ were analyzed by competitive binding ELISA as described previously (22).

Flow cytometry. Integrin expression on the cell lines was determined as previously described (24).

Cell binding and internalization. A cell suspension (3.75×10^6 cells) was incubated with the radiotracer (0.2 μCi) in serum-free medium (pH 7.2, 100 μL). For each radiotracer, the cell lines were assayed concurrently ($n = 4$ samples per cell line per time point). The fraction of bound radioactivity was determined with a γ-counter (cell pellet versus supernatant). To determine the fraction of internalized radioactivity, the cells were then treated with acidic wash buffer [0.2 mol/L sodium acetate, 0.5 mol/L sodium chloride (pH 2.5), 4°C] to release surface-bound activity (25). The internalized fraction was determined with a γ-counter (cell pellet versus radioactivity released into supernatant).

Xenograft cell lines and animal model. All animal studies were carried out using male athymic nude mice (*nu/nu*; Charles River Laboratories) following approved protocols. DX3puroβ6 ($\alpha_v\beta_6$ positive) and DX3puro (control) cells were injected s.c. ($n = 20$ mice; 3×10^6 cells/cell line in 100 μL serum-free DMEM; Invitrogen) on opposite flanks in the shoulder region, as described previously (22). BxPC-3 cells were injected s.c. ($n = 30$ mice; 1.5×10^6 cells in 100 μL 1:1 serum-free DMEM/Matrigel HC; BD Biosciences) in the left shoulder region. Studies commenced once tumors had reached a diameter of ~0.5 cm.

Biodistribution studies. Radiotracers (~15–30 μCi) in saline/PBS (150–200 μL) were injected, and data were analyzed as previously described ($n = 3$ per time point; ref. 22).

MicroPET imaging studies. The [^{18}F]FBA peptides or [^{18}F]FDG (~120–230 μCi) in saline/PBS (100–200 μL) were injected as previously described ($n = 3$ per time point; ref. 22). Two animals were imaged side-by-side in a feet-first prone position. For blocking studies, the [^{19}F]FBA peptide (30 mg/kg as 10 mg/mL solution in saline) was injected 10 min before the radiotracer. Imaging data were collected and analyzed as previously described (22, 26).

Standard uptake values (SUV) were computed by dividing the activity concentration in each voxel by the injected dose and then multiplying by the weight of the animal (26). Maximum intensity projection (MIP) images were created by collapsing across one dimension with the maximum value in each column of voxels.

Autoradiography studies. Frozen tissue slices (tumor and surrounding tissue, 50 μm) in freezing medium (Tissue-Tek, Sakura Finetek) were exposed to a storage phosphor screen (GE Healthcare) overnight. The screen was read at a 50-μm resolution using a Storm 860 phosphorimager (GE Healthcare).

Statistical analysis. The data are reported as mean ± SD. Two-tailed Student's t tests were performed to evaluate statistical significance. $P < 0.05$ was considered significant. In plots, the SD is smaller than the size of the symbol for some data points.

Results

PEGylated peptide ligands for $\alpha_v\beta_6$. PEGylated A20FMDV2 variants were compared by ELISA to the established $\alpha_v\beta_6$ peptide ligand FBA-A20FMDV2 (Fig. 1). They exhibited IC_{50} of 3 to 6 nmol/L, similar to FBA-A20FMDV2. Inhibition of binding by the natural ligands to integrins $\alpha_v\beta_3$, $\alpha_v\beta_5$, $\alpha_5\beta_1$, and $\alpha_{IIb}\beta_3$ required at least >1,000-fold higher concentrations of peptide (IC_{50} >10 μmol/L), indicating that introduction of the PEG moieties did not have a deleterious effect on $\alpha_v\beta_6$ affinity and selectivity of A20FMDV2.

Integrin $\alpha_v\beta_6$ expression in human pancreatic cancer cell lines. Seven cell lines were screened by flow cytometry for $\alpha_v\beta_6$ expression (Fig. 2). For reference, the melanoma cell line DX3puroβ6, stably transduced to express $\alpha_v\beta_6$, and its paired control line DX3puro, lacking expression of $\alpha_v\beta_6$, were analyzed as positive and negative controls, respectively; both of these cell lines express similar levels of other integrins, including $\alpha_v\beta_3$, $\alpha_v\beta_5$, and $\alpha_5\beta_1$ (22). BxPC-3 and Capan-2 showed high $\alpha_v\beta_6$ expression levels comparable with that of the positive control DX3puroβ6. Capan-1 and L3.3 showed intermediate expression of $\alpha_v\beta_6$, whereas MIA-PaCa2, Panc-1, and BCL-2cl9 showed expression levels equivalent to that of the negative control DX3puro.

Cell binding and internalization. Binding of the radiotracers [^{18}F]FBA-(PEG$_{28}$)$_n$-A20FMDV2 ($n = 0, 1, 2$; Supplementary Fig. S1 and S2; ref. 22) to DX3puroβ6, DX3puro, and BxPC-3 cell lines was strongly dependent on the expression of $\alpha_v\beta_6$ by the cells and on the presence of a PEG unit in the radiotracer (Fig. 3). Whereas <2% of any radiotracer bound to the $\alpha_v\beta_6$-negative DX3puro within 1 hour (Fig. 3*A*), 5.3 ± 0.8% and 9.7 ± 1.2% of [^{18}F]FBA-A20FMDV2 bound to the $\alpha_v\beta_6$-expressing DX3puroβ6 and BxPC-3 cell lines, respectively. For [^{18}F]FBA-PEG$_{28}$-A20FMDV2, the binding levels increased significantly to 73.5 ± 1.3% and 68.9 ± 0.2%, respectively. Similarly, [^{18}F]FBA-(PEG$_{28}$)$_2$-A20FMDV2 showed markedly elevated binding levels of 38.5 ± 1.7% and 25.8 ± 0.6%, respectively. Approximately two-thirds of the bound radioactivity was internalized in the $\alpha_v\beta_6$-expressing cell lines in the case of the two PEGylated radiotracers, whereas less than half of the bound [^{18}F]FBA-A20FMDV2 was internalized. Incubation in the presence of excess nonradioactive [^{19}F]FBA-PEG$_{28}$-A20FMDV2 (≥1μmol/L) completely abrogated binding of the radiotracer to DX3puroβ6 cells (Supplementary Fig. S3).

Figure 3*B* illustrates the rapid cell binding of radiotracer. Within 1 minute, approximately one quarter of [^{18}F]FBA-PEG$_{28}$-A20FMDV2 bound to DX3puroβ6 and BxPC-3 (30.5 ± 2.7% and 24.5 ± 1.2%, respectively). Binding levels approached their maximum within 15 to 30 minutes and then remained steady. When the two cell lines were incubated with [^{18}F]FBA-PEG$_{28}$-A20FMDV2 for 1 hour in the presence of LAP, the radiotracer was able to efficiently compete for binding; binding levels in presence of 5 nmol/L LAP remained at ≥75% of those observed under LAP-free conditions (Supplementary Fig. S4).

[^{18}F]FBA-(PEG$_{28}$)$_n$-A20FMDV2 ($n = 0, 1, 2$) biodistribution in the DX3puro/DX3puroβ6 model. Initial *in vivo* evaluation of [^{18}F]FBA-PEG$_{28}$-A20FMDV2 and [^{18}F]FBA-(PEG$_{28}$)$_2$-A20FMDV2 was performed using our previously described mouse model bearing the paired human xenografts of DX3puroβ6 ($\alpha_v\beta_6$ positive) and DX3puro ($\alpha_v\beta_6$ negative; Supplementary Table S1). Whereas uptake of both PEGylated radiotracers in the target tissue at 1 hour postinjection was slightly below the level previously seen for the non-PEGylated [^{18}F]FBA-A20FMDV (22), the introduction of the PEG unit(s) resulted in excellent retention of radioactivity in the $\alpha_v\beta_6$-positive tumor ([^{18}F]FBA-PEG$_{28}$-A20FMDV2, 1 hour: 0.49 ± 0.12% ID/g, 4 hours: 0.49 ± 0.04% ID/g; [^{18}F]FBA-(PEG$_{28}$)$_2$-A20FMDV2, 1 hour: 0.52 ± 0.09% ID/g, 4 hours: 0.54 ± 0.08% ID/g; compared with [^{18}F]FBA-A20FMDV2, 1 hour: 0.66 ± 0.09% ID/g,

Published OnlineFirst June 23, 2009; DOI: 10.1158/0008-5472.CAN-08-4410

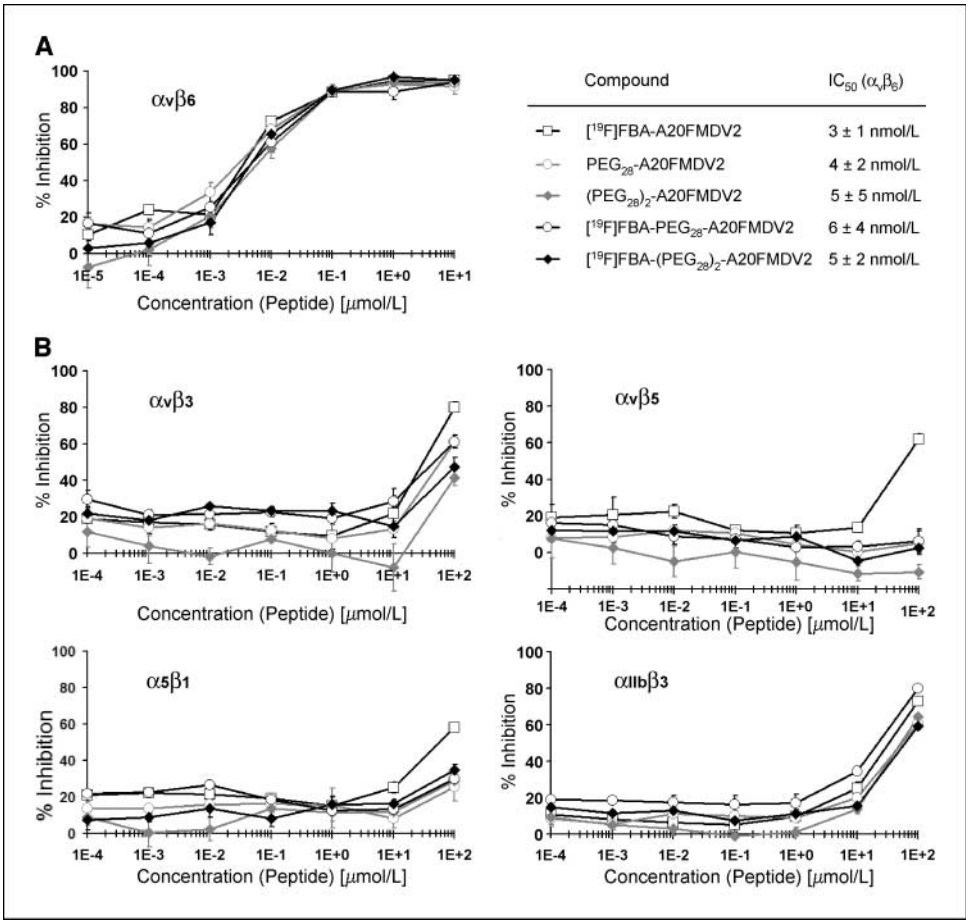

Figure 1. Use of ELISA to measure the effect of introducing PEG groups with and without [^{19}F]FBA on the ability of A20FMDV2 to inhibit binding of biotinylated natural ligands to immobilized integrins. Peptides and biotinylated ligands were mixed and allowed to compete during 1 h for binding to integrin $\alpha_v\beta_6$ (*A*) and $\alpha_v\beta_3$, $\alpha_v\beta_5$, $\alpha_5\beta_1$, or $\alpha_{IIb}\beta_3$ (*B*). Ligands used were biotinylated fibronectin ($\alpha_v\beta_6$, $\alpha_5\beta_1$), biotinylated vitronectin ($\alpha_v\beta_3$, $\alpha_v\beta_5$), or biotinylated fibrinogen ($\alpha_{IIb}\beta_3$). Plots represent triplicate experiments at each concentration. *Points*, percentage of inhibition; *bars*, SD. IC_{50} values were derived from *A*.

4 hours: 0.06 ± 0.00% ID/g). A comparison of the uptake in the two xenografts consistently showed preferential uptake in the $\alpha_v\beta_6$-positive xenograft over the $\alpha_v\beta_6$-negative xenograft, particularly for the PEGylated radiotracers. Whereas [^{18}F]FBA-A20FMDV resulted in a 4.3:1 maximal $\alpha_v\beta_6$-positive/$\alpha_v\beta_6$-negative ratio, ratios of 8.0:1 and 9.2:1 were seen for [^{18}F]FBA-PEG_{28}-A20FMDV2 and [^{18}F]FBA-$(PEG_{28})_2$-A20FMDV2, respectively (for *P* values, see Supplementary Table S1).

[^{18}F]FBA-$(PEG_{28})_n$-A20FMDV2 (*n* = 0, 1, 2) biodistribution in the $\alpha_v\beta_6$-endogenous BxPC-3 model. The feasibility of $\alpha_v\beta_6$-targeted pancreatic tumor detection *in vivo* was evaluated in the BxPC-3 mouse model (Fig. 4; Supplementary Table S1). For [^{18}F]FBA-A20FMDV2 initial uptake in and washout from the BxPC-3 xenograft (1 hour: 0.69 ± 0.19% ID/g, 4 hours: 0.12 ± 0.03% ID/g) were similar to those seen in the DX3puroβ6 xenograft (1 hour: 0.66 ± 0.09% ID/g, 4 hours: 0.06 ± 0.00% ID/g). By contrast, for both of the PEGylated radiotracers uptake in the BxPC-3 xenograft 1 hour after injection was three to four times higher than in the DX3puroβ6 xenograft, combined with excellent retention ([^{18}F]FBA-PEG_{28}-A20FMDV2, 1 hour: 1.85 ± 0.44% ID/g, 4 hours: 1.48 ± 0.04% ID/g; [^{18}F]FBA-$(PEG_{28})_2$-A20FMDV2, 1 hour: 1.57 ± 0.25% ID/g, 4 hours: 2.08 ± 0.37% ID/g). Autoradiography images obtained for the PEGylated radiotracers of BxPC-3 xenografts 1 hour after injection also showed preferential, tumor-specific uptake (Fig. 5).

Renal clearance was the major route of elimination for all three radiotracers (Fig. 4 and data not shown). High-performance liquid chromatography (HPLC) analyses of urine samples showed three metabolites for [^{18}F]FBA-A20FMDV2 and one major metabolite for each of the PEGylated radiotracers. Distribution of the radiotracers in healthy tissues generally depended on the number of PEG units present (Fig. 4; Supplementary Table S1). Non-PEGylated [^{18}F]FBA-A20FMDV2 was washed out efficiently from all tissues examined, with gall bladder and kidneys containing the highest levels of radioactivity. By contrast, the di-PEGylated [^{18}F]FBA-$(PEG_{28})_2$-A20FMDV2 was generally retained throughout, most notably in the kidneys (~42% ID/g); only blood showed clearing of radioactivity. Pharmacokinetics of the mono-PEGylated [^{18}F]FBA-PEG_{28}-A20FMDV2 in healthy tissues compared favorably to the di-PEGylated radiotracer, resulting in a desirable clearing behavior resembling that observed for the non-PEGylated compound in healthy tissues; highest levels of radioactivity were detected in the kidneys and the gall bladder.

The BxPC-3/blood ratio remained relatively low for [^{18}F]FBA-A20FMDV2 (1 hour: 3.3:1, 4 hours: 7.0:1) and the BxPC-3/muscle ratio only reached statistically significant levels at the 4-hour time point (1 hour: 1.3:1, $P = 0.38$; 4 hours: 2.5:1, $P = 0.02$) because of more rapid washout from healthy tissues than from the tumor (Fig. 4, Supplementary Table S1). By comparison, improved BxPC-3/muscle ratios were seen for [^{18}F]FBA-PEG_{28}-A20FMDV2 (1 hour: 2.5:1, 4 hours: 3.6:1) and [^{18}F]FBA-$(PEG_{28})_2$-A20FMDV2 (1 hour: 4.1:1, 4 hours: 4.4:1), along with significantly higher BxPC-3/blood ratios ([^{18}F]FBA-PEG_{28}-A20FMDV2, 1 hour: 11.8:1, 4 hours: 47.9:1; [^{18}F]FBA-$(PEG_{28})_2$-A20FMDV2, 1 hour: 9.0:1, 4 hours: 150:1),

Published OnlineFirst June 23, 2009; DOI: 10.1158/0008-5472.CAN-08-4410

reflecting the improved retention of these radiotracers in the BxPC-3 tumor.

Importantly, levels of radioactivity in the BxPC-3 tumor were at least 4-fold higher than those for the pancreas itself for all radiotracers at all time points measured (Supplementary Table S1). For [^{18}F]FBA-A20FMDV2, the BxPC-3/pancreas ratio rose to 9.5:1 at 4 hours postinjection due to the more efficient washout from the pancreas than from the tumor. On the other hand, because of retention of [^{18}F]FBA-$(PEG_{28})_2$-A20FMDV2 in healthy pancreas, the BxPC-3/pancreas ratio for this radiotracer remained nearly unchanged throughout (1 hour: 5.6:1, 4 hours: 4.4:1). [^{18}F]FBA-PEG_{28}-A20FMDV2 exhibited good retention in the tumor together with efficient washout from the pancreas (and other healthy tissues), resulting in a steadily increasing BxPC-3/pancreas ratio (1 hour: 4.2:1, 4 hours: 23.6:1). In summary, the mono-PEGylated [^{18}F]FBA-PEG_{28}-A20FMDV2 had the most favorable pharmacokinetic characteristics.

MicroPET imaging of the $\alpha_v\beta_6$-endogenous BxPC-3 pancreatic cancer model. Figure 5*A* depicts representative coronal and transaxial MIPs obtained with the three [^{18}F]FBA peptide tracers and with [^{18}F]FDG (1 hour postinjection). Tumor uptake was compared based on maximum SUVs (SUV_{max}; n = 3 animals).

The observations made for the peptide radiotracers during microPET imaging paralleled the results seen in the biodistribution study with preferential uptake noted in the tumor along with major uptake in kidneys, bladder (urine), and, for [^{18}F]FBA-A20FMDV2, gall bladder. [^{18}F]FBA-A20FMDV2 showed moderate initial tumor uptake and significant washout over time (SUV_{max}, 15 minutes: 0.50 $\pm$ 0.22, 1 hour: 0.22 $\pm$ 0.11; 4 hours: < 0.05). [^{18}F]FBA-$(PEG_{28})_2$-A20FMDV2 showed improved uptake and retention in the tumor (SUV_{max}, 15 minutes: 0.99 $\pm$ 0.18, 1 hour: 0.79 $\pm$ 0.24, 4 hours: 0.59 $\pm$ 0.20), along with significant renal retention. [^{18}F]FBA-PEG_{28}-A20FMDV2 combined favorable tumor uptake characteristics (SUV_{max}, 15 minutes: 1.07 $\pm$ 0.29, 1 hour: 0.91 $\pm$ 0.25, 4 hours: 0.63 $\pm$ 0.12) with good renal clearance.

Administration of nonradioactive [^{19}F]FBA-PEG_{28}-A20FMDV2 (30 mg/kg) 10 minutes before the corresponding [^{18}F]FBA peptide greatly reduced BxPC-3 tumor uptake [$\Delta(SUV_{max}) = -77\%$; Fig. 5*B*]. Similar results were obtained for [^{19}F]FBA-$(PEG_{28})_2$-A20FMDV2 (30 mg/kg)/[^{18}F]FBA-peptide [$\Delta(SUV_{max}) = -60\%$; Fig. 5*C*]. Interestingly, [^{18}F]FBA-PEG_{28}-A20FMDV2 and [^{18}F]FBA-$(PEG_{28})_2$-A20FMDV2 were retained in the mouse oral cavity in scans without prior administration of nonradioactive FBA-peptide, suggesting that there may be limited expression of $\alpha_v\beta_6$ (27).

MicroPET scans obtained with [^{18}F]FDG revealed an SUV_{max} of 0.62 $\pm$ 0.13 in the BxPC-3 tumor (1 hour postinjection, n = 3; Fig. 5*A*). This level of tumor uptake is relatively low for [^{18}F]FDG, and it was within the range observed for the surrounding tissue ($\sim$0.4–0.8). Thus, whereas the [^{18}F]FBA peptide tracers clearly revealed the BxPC-3 tumor *in vivo*, [^{18}F]FDG did not.

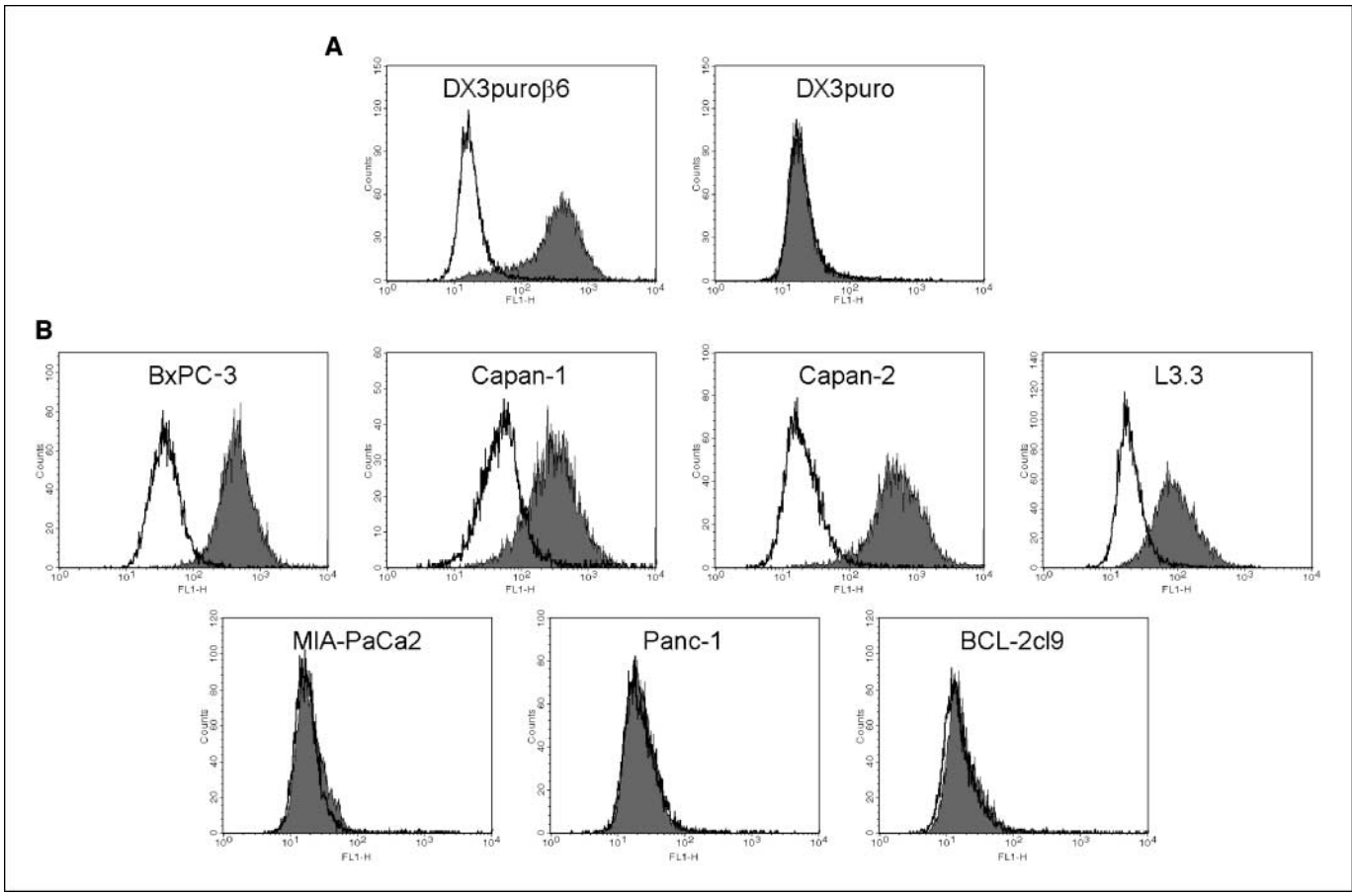

Figure 2. Expression of integrin $\alpha_v\beta_6$ by cell lines used in this study. Flow cytometry histogram plots for an $\alpha_v\beta_6$-positive (DX3puroβ6) and an $\alpha_v\beta_6$-negative (DX3puro) cell line (*A*) and seven pancreatic cancer cell lines (*B*) were obtained. Levels of $\alpha_v\beta_6$ (*gray histograms*) were determined using the integrin $\alpha_v\beta_6$-specific antibody 10D5. Mouse IgG (MOPC 21; *white histograms*) was used as antibody control.

Published OnlineFirst June 23, 2009; DOI: 10.1158/0008-5472.CAN-08-4410

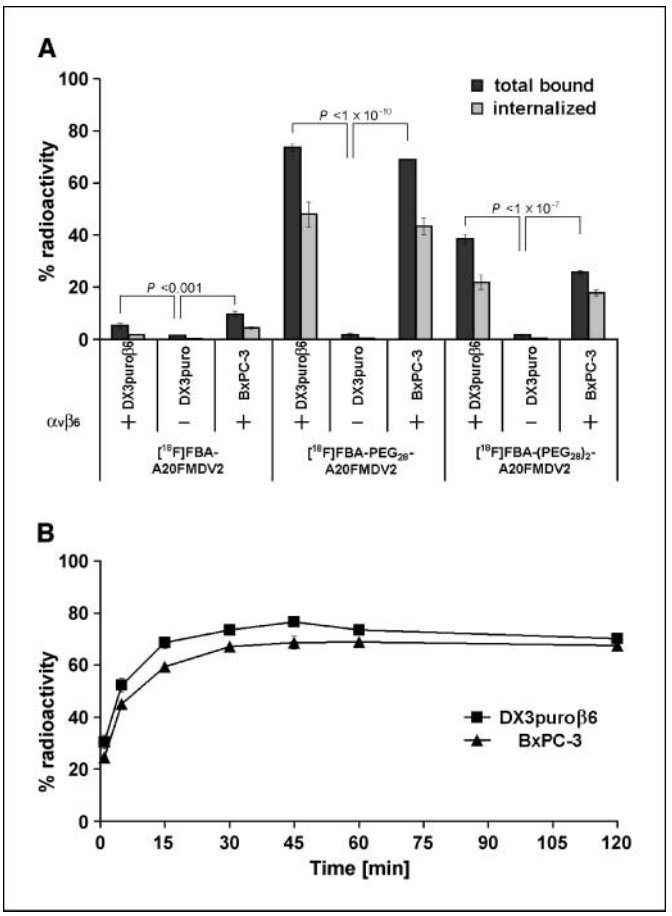

Figure 3. *A,* binding and internalization of [^{18}F]FBA-A20FMDV2, [^{18}F]FBA-PEG$_{28}$-A20FMDV2, and [^{18}F]FBA-(PEG$_{28}$)$_2$-A20FMDV2 for DX3puroβ6, DX3puro, and BxPC-3 cell lines after a 1-h incubation: *dark gray columns,* total bound radioactivity; *light gray columns,* internalized. *B,* binding kinetics of [^{18}F]FBA-PEG$_{28}$-A20FMDV2 for the $\alpha_v\beta_6$-positive cell lines DX3puroβ6 and BxPC-3. Plots represent quadruplicate experiments with 3.75×10^6 cells at each condition or time point, respectively. *Filled columns, points*, percentage of radioactivity in cell sample; *bars,* SD.

Discussion

The integrin $\alpha_v\beta_6$ has been identified as a prognostic biomarker for cancer of the colon, cervix, lung, and stomach (10–12, 21). In addition, $\alpha_v\beta_6$ is reported to be expressed by many other types of carcinoma (13, 19) whereas corresponding normal tissue is weak or negative. Thus, $\alpha_v\beta_6$ represents an excellent target for imaging and therapy of carcinoma. We previously showed the ability to selectively image $\alpha_v\beta_6$-expressing tumors *in vivo* using the PET radiotracer [^{18}F]FBA-A20FMDV2 (22). While targeted imaging was achieved, low uptake and poor retention in the target tissue, together with metabolic instability, limited its general utility, leading us to explore strategies to improve pharmacokinetics. As introduction of PEG moieties (PEGylation) generally increases biological half-life, metabolic stability, and tumor-uptake (28, 29), we generated two variants of A20FMDV2 that included PEG moieties on the N-terminus of the peptide. These PEGylated variants of [^{18}F]FBA-A20FMDV2 were examined and compared with the parent compound. Monodisperse PEG polymers of moderate molecular weight [Fw(PEG$_{28}$) = 1.3 kDa] are short enough to be compatible with solid-phase chemistries yet large enough to be expected to approach a range with some beneficial *in vivo* (pharmacokinetic) properties. Additionally, owing to the monodisperse nature of the polymer, the final product is obtained as a single compound, allowing for precise characterization and batch-to-batch reproducibility, in contrast to mixtures containing polymer chains of different lengths encountered with the larger PEG products available.

As presented here, initial *in vitro* evaluation by ELISA indicated unchanged, high $\alpha_v\beta_6$-specificity for the PEGylated compounds (Fig. 1). Further binding experiments with the DX3puroβ6 and DX3puro cell lines showed strong, $\alpha_v\beta_6$-specific and PEG-dependent binding to the receptor expressed on cells in the presence of other related integrins (including $\alpha_v\beta_3$, $\alpha_v\beta_5$, and $\alpha_5\beta_1$; Fig. 3). *In vivo* studies also showed improved, $\alpha_v\beta_6$-targeted PEG-dependent tumor retention in the DX3puroβ6/DX3puro model (Supplementary Table S1). Taken together, these data confirmed our initial expectations for the two new PEGylated radiotracers, [^{18}F]FBA-PEG$_{28}$-A20FMDV2 and [^{18}F]FBA-(PEG$_{28}$)$_2$-A20FMDV2.

The DX3puroβ6/DX3puro melanoma cancer model was generated by viral transduction of human β6 into human melanoma cells. To examine a model more closely resembling the actual human disease, we sought a cancer wherein the expression of $\alpha_v\beta_6$ was relevant to the disease and for which cell lines that had endogenous expression of $\alpha_v\beta_6$ existed; we chose to investigate pancreatic cancer. Sipos and colleagues (20) reported, as part of a study of gastroenteropancreatic adenocarcinomas, that $\alpha_v\beta_6$ expression was strongest in PDACs. Thus, of the 34 human PDAC samples analyzed, 32 (94%) received the maximum score (the mean score was 2.8/3.0, with none of the other carcinomas receiving a score over 1.5). These observations make $\alpha_v\beta_6$ a very appealing target for selective *in vivo* detection of pancreatic cancer. The possibility of detecting primary tumors and metastases earlier by imaging $\alpha_v\beta_6$ and, thus, directing therapy sooner may improve upon the very poor prognosis of this disease. In addition, recent studies associate strong expression of $\alpha_v\beta_6$ with poor prognosis (for colon, lung, cervical, and stomach cancers; refs. 10–12, 21), so the relevance of our data is not restricted only to pancreatic cancer.

As shown here by flow cytometry (Fig. 2), many common pancreatic carcinoma cell lines exhibit an $\alpha_v\beta_6$ profile that reflects expression seen for PDAC in the clinic (20). *In vitro* cell-binding assays showed that [^{18}F]FBA-PEG$_{28}$-A20FMDV2 performed equally well with the endogenously $\alpha_v\beta_6$-expressing pancreatic BxPC-3 cell line and the transduced $\alpha_v\beta_6$-expressing DX3puroβ6 cell line, showing rapid and high binding together with significant internalization (Fig. 3). Contrary to conditions in the *in vivo* environment, these assays were performed in the absence of natural ligands competing for binding to $\alpha_v\beta_6$. We, therefore, sought to further show their relevance as predictors for *in vivo* performance by carrying out a binding assay in the presence of a biologically relevant $\alpha_v\beta_6$ ligand. LAP was chosen as it binds to $\alpha_v\beta_6$ with high affinity and has significance in the context of tumor biology (13, 18, 30). In association with TGFβ, particularly TGFβ1, LAP binds to $\alpha_v\beta_6$, thereby affecting signaling pathways understood to play significant roles in tumor development (18, 30). We found that, even in the presence of 5 nmol/L LAP, the radiotracer, present at subpicomolar levels, was still able to efficiently bind to the cells (at $\geq$75% of binding observed under LAP-free conditions; Supplementary Fig. S4). The feasibility of evaluating $\alpha_v\beta_6$-specific *in vivo* imaging radiotracers for pancreatic carcinoma was shown in a mouse model bearing

Published OnlineFirst June 23, 2009; DOI: 10.1158/0008-5472.CAN-08-4410

BxPC-3 xenografts. In microPET images, the BxPC-3 tumors were clearly identifiable throughout. These data confirm that selective *in vivo* imaging of $\alpha_v\beta_6$-expressing cancers is possible with cancers that endogenously express $\alpha_v\beta_6$ and not only those engineered to express it. Importantly for pancreatic imaging, the best pharmacokinetic behavior was observed for [^{18}F]FBA-PEG$_{28}$-A20FMDV2, resulting in the highest tumor/pancreas ratio (>23:1; 4 hours), making this radiotracer a promising lead compound for *in vivo* detection.

Close examination of the biodistribution data revealed that introduction of the second PEG unit was not beneficial. Simply modifying from [^{18}F]FBA-PEG$_{28}$-A20FMDV2 to [^{18}F]FBA-(PEG$_{28}$)$_2$-A20FMDV2 resulted only in a slight increase in tumor uptake, whereas, concurrently, washout of radioactivity from healthy tissue (except blood) was suppressed over the time span examined; particularly notable are the high and constant levels of radioactivity in the kidneys (Fig. 4). PET images also showed that [^{18}F]FBA-PEG$_{28}$-A20FMDV2 outperformed [^{18}F]FBA-(PEG$_{28}$)$_2$-A20FMDV2; it showed slightly higher uptake (SUV$_{max}$) together with better BxPC-3/background ratios, largely due to preferential clearing of nonspecifically bound activity (Fig. 5). Thus, in this study, [^{18}F]FBA-PEG$_{28}$-A20FMDV2 seemed to have the best balance of $\alpha_v\beta_6$-dependent tumor uptake and a suitable rate of clearance from healthy tissues, including the pancreas. The high retention of [^{18}F]FBA-(PEG$_{28}$)$_2$-A20FMDV2 in healthy tissues, caused by introduction of the second PEG unit, had not been predicted. These observations seem to stand in contrast to the common belief that renal clearance remains highly efficient for compounds bearing small PEG units (under ~30 kDa; refs. 28, 29). Despite the comparatively small PEG units used in this study, the PEGylation of A20FMDV2 seemed to result in an "enhanced permeation and retention" effect toward the BxPC-3 tumors along with some improved radiotracer stability (29). Positive effects of PEGylation on the *in vivo* stability of pharmaceuticals are generally recognized (28). Likewise, in our study, only one major radioactive metabolite was found in HPLC samples of urine collected 1 hour after injection of [^{18}F]FBA-PEG$_{28}$-A20FMDV2 or [^{18}F]FBA-(PEG$_{28}$)$_2$-A20FMDV2, whereas the non-PEGylated analogue had yielded three equally large metabolite signals (22). However, because the cell-based assays showed very rapid binding (~25% of [^{18}F]FBA-PEG$_{28}$-A20FMDV2 bound to BxPC-3 within 1 minute; Fig. 3*B*) and significant, PEG-dependent internalization (approximately two thirds of bound activity were internalized at 1 hour; Fig. 3*A*), delivery efficiency to the target likely was of principal importance for these radiotracers, provided that radioactive metabolites were rapidly cleared from the body, as observed particularly for [^{18}F]FBA-PEG$_{28}$-A20FMDV2. Taken together, these data suggest that rapid binding and internalization of the PEGylated radiotracers in cells are key to increased uptake and retention in the tumors. That being said, a detailed characterization of metabolites and further modification of the radiotracers remain of interest. They include selective deletion of redundant amino acids and replacement with unnatural amino acids in conjunction with multimeric radiotracers and incorporation of branched PEG. These approaches have already been successful in improving the pharmacokinetics of tracers for integrin $\alpha_v\beta_3$ (28, 31, 32).

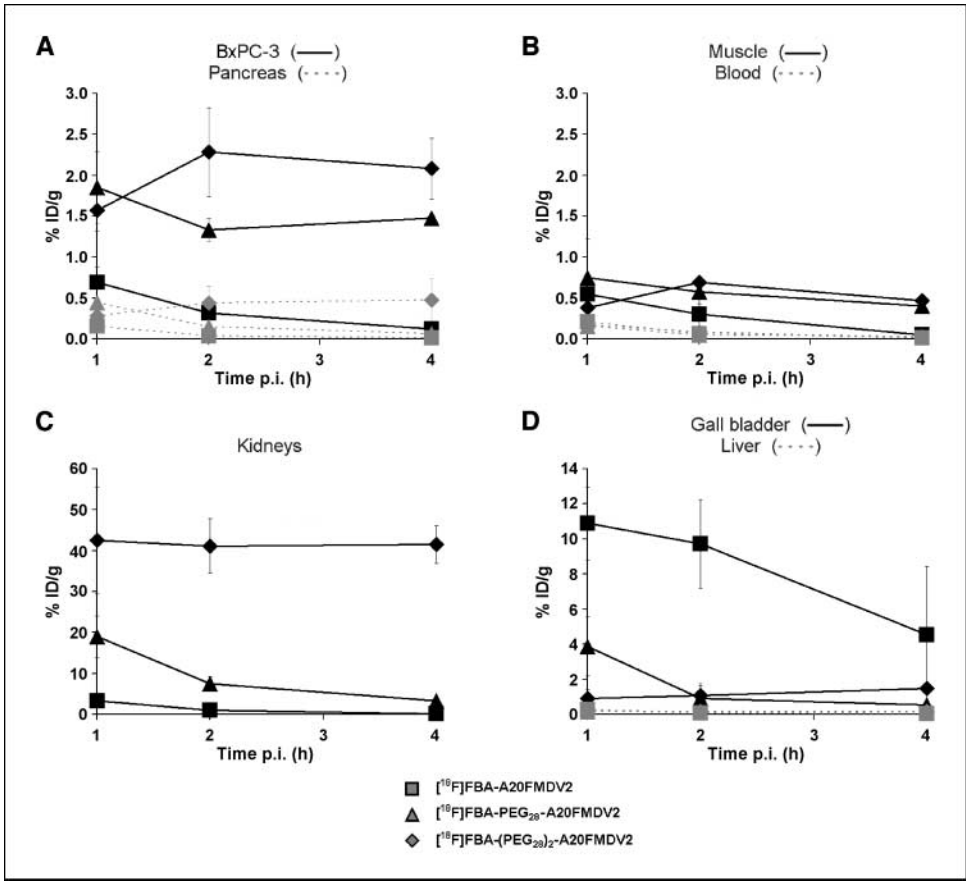

Figure 4. Evaluation of pharmacokinetics. Biodistribution data for [^{18}F]FBA-A20FMDV2, [^{18}F]FBA-PEG$_{28}$-A20FMDV2, and [^{18}F]FBA-(PEG$_{28}$)$_2$-A20FMDV2 in BxPC-3 tumors and healthy tissues obtained in male nude mice, expressed as decay corrected percentage of injected dose per gram of tissue (% ID/g ± SD). *Points,* % ID/g; *bars,* SD. Data were obtained 1, 2, and 4 h after i.v. injection of the radiotracer (n = 3 per time point per radiotracer) for the BxPC-3 tumor and pancreas (*A*), muscle and blood (*B*), kidneys (*C*), and gall bladder and liver (*D*). For all three radiotracers and time points, the corresponding differences in uptake in BxPC-3 versus pancreas were statistically significant (*A*). For P values, see Supplementary Table S1.

Published OnlineFirst June 23, 2009; DOI: 10.1158/0008-5472.CAN-08-4410

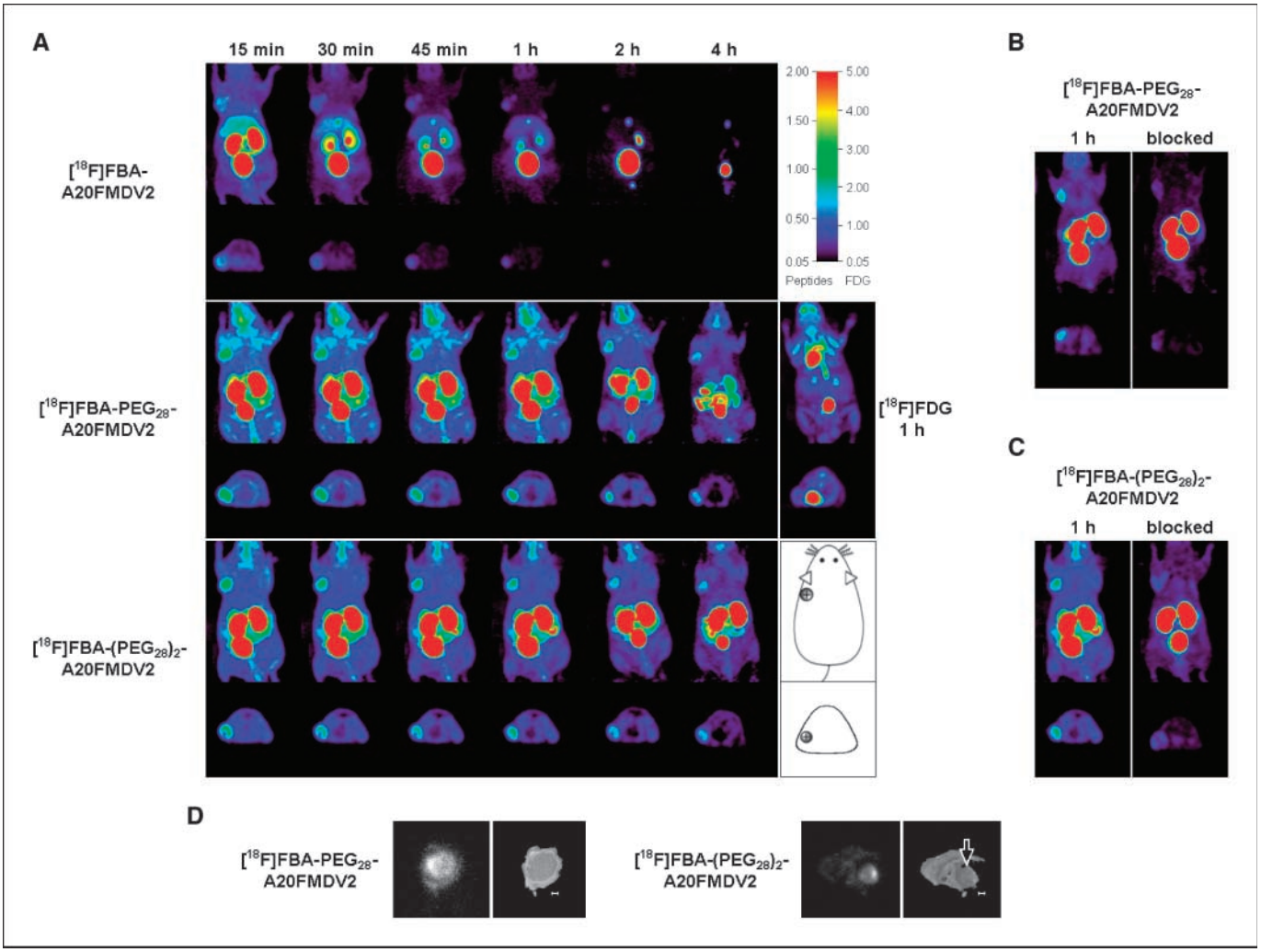

Figure 5. *In vivo* evaluation of radiotracers in BxPC-3 xenograft–bearing male nu/nu mice using microPET (*A–C*), as well as autoradiography (*D*). *A,* representative coronal and transaxial MIPs obtained in the same animal after bolus injection of the radiotracers into the tail vein. For all [^{18}F]FBA peptides, the first four panels were obtained as part of a dynamic 4 × 15 min scan started 15 min after injection. Subsequent panels depict 15-min scans at 2 and 4 h after injection, respectively, with the animal having been awake between scans. The radioactivity was allowed to clear fully between injections of the different radiotracers. *A* also depicts MIPs of an [^{18}F]FDG scan (*middle right*; same animal). The location of the tumor is indicated in the diagram (*bottom right*). *B,* effect of prior administration of [^{19}F]FBA-PEG$_{28}$-A20FMDV2. Images obtained after administration of [^{18}F]FBA-PEG$_{28}$-A20FMDV2 only (*left*), and images obtained after first administering nonradioactive [^{19}F]FBA-PEG$_{28}$-A20FMDV2 (i.v., 30 mg/kg) 10 min before [^{18}F]FBA-PEG$_{28}$-A20FMDV2 (*right*). Both images were obtained 1 h after administration of the radiotracer. *C,* same as *B* using [^{19}F]FBA-(PEG$_{28}$)$_2$-A20FMDV2/[^{18}F]FBA-(PEG$_{28}$)$_2$-A20FMDV2 in same animal as in *A. D,* autoradiography images of tumor slices obtained from animals sacrificed 1 h after injection of ~500 μCi [^{18}F]FBA-PEG$_{28}$-A20FMDV2 or [^{18}F]FBA-(PEG$_{28}$)$_2$-A20FMDV2, and corresponding photographic images (*right*). *Bars,* 0.1 cm; *arrow,* location of tumor.

Paralleling the *in vitro* blocking studies with the $\alpha_v\beta_6$-expressing cell lines, *in vivo* blocking experiments using the nonradioactive analogues showed a significant reduction of uptake in the BxPC-3 tumors. Before the blocking experiments, the animals were also evaluated by [^{18}F]FDG-PET, the standard radiotracer for PET imaging. Significantly, [^{18}F]FDG failed in all animals to detect the BxPC-3 tumors. In the clinical setting, [^{18}F]FDG is by far the most widely used PET radiotracer for the detection of many cancers, including pancreatic cancer, despite the risk of false positive (e.g., pancreatitis) or false negative (e.g., low GLUT-1 glucose transporter expression in tumor; hyperglycemic patient) diagnosis. Thus, our observation parallels findings from the clinical setting wherein [^{18}F]FDG is estimated to miss over one third of all pancretic malignancies (and about half of the lesions smaller than 1 cm; refs. 6, 8, 33).

Better understanding of the biology of pancreatic cancer (34) and improved early, more accurate diagnosis are sorely needed. By combining detailed anatomical information with functional metabolic information, [^{18}F]FDG-PET/CT has shown some promise (5, 6, 8, 33). However, the use of [^{18}F]FDG as radiotracer does not take advantage of the molecular biological differences of tumors beyond their increased (glucose) metabolism. The integrin $\alpha_v\beta_6$ is expressed strongly by most human pancreatic cancers (20) and is likely to be a prognostic indicator for this cancer. Therefore, it is clear that targeted *in vivo* imaging of $\alpha_v\beta_6$ will be a major improvement for preoperative staging and monitoring response to treatment for this lethal malignancy in humans. Using a metabolic probe ([^{18}F]FDG) in conjunction with receptor-specific radiotracers in PET/CT could provide crucial additional information, particularly for occult disease. In a step

Published OnlineFirst June 23, 2009; DOI: 10.1158/0008-5472.CAN-08-4410

toward making this a clinical reality, we have shown that [^{18}F]FBA-PEG$_{28}$-A20FMDV2 holds promise for $\alpha_v\beta_6$-specific tumor imaging.

Disclosure of Potential Conflicts of Interest

No potential conflicts of interest were disclosed.

Acknowledgments

Received 11/21/08; revised 4/29/09; accepted 5/8/09; published OnlineFirst 6/23/09.

Grant support: NIH grant R21 CA107792.

The costs of publication of this article were defrayed in part by the payment of page charges. This article must therefore be hereby marked *advertisement* in accordance with 18 U.S.C. Section 1734 solely to indicate this fact.

We thank J. Choi, D.L. Kukis, L. Planutyte, C.D. Griesemer, J.Y. Fung, and S.V. Rendig for excellent technical support.

References

1. Alavi A, Kung JW, Zhuang HM. Implications of PET based molecular imaging on the current and future practice of medicine. Semin Nucl Med 2004;34:56–69.

2. Keogan MT, Tyler D, Clark L, et al. Diagnosis of pancreatic carcinoma: role of FDG PET. Am J Roentgenol 1998;171:1565–70.

3. Rose DM, Delbeke D, Beauchamp RD, et al. ^{18}Fluorodeoxyglucose positron emission tomography in the management of patients with suspected pancreatic cancer. Ann Surg 1999;229:729–38.

4. Czernin J, Allen-Auerbach M, Schelbert HR. Improvements in cancer staging with PET/CT: literature-based evidence as of September 2006. J Nucl Med 2007;48:78S–88S.

5. Heinrich S, Goerres GW, Schäfer M, et al. Positron emission tomography/computed tomography influences on the management of resectable pancreatic cancer and its cost-effectiveness. Ann Surg 2005;242:235–43.

6. Schöder H, Gönen M. Screening for cancer with PET and PET/CT: potential and limitations. J Nucl Med 2007;48:4S–18S.

7. Blodgett TM, Meltzer CC, Townsend DW. PET/CT: form and function. Radiology 2007;242:360–85.

8. Parsons CM, Sutcliffe JL, Bold RJ. Preoperative evaluation of pancreatic cancer. J Hepato Biliary Pancreatic Surg 2008;15:429–35.

9. Beer AJ, Haubner R, Goebel M, et al. Biodistribution and pharmacokinetics of the $\alpha_v\beta_3$-selective tracer ^{18}F-galacto-RGD in cancer patients. J Nucl Med 2005;46:1333–41.

10. Bates RC, Bellovin DI, Brown C, et al. Transcriptional activation of integrin β_6 during the epithelial-mesenchymal transition defines a novel prognostic indicator of aggressive colon carcinoma. J Clin Invest 2005;115:339–47.

11. Hazelbag S, Kenter GG, Gorter A, et al. Overexpression of the $\alpha_v\beta_6$ integrin in cervical squamous cell carcinoma is a prognostic factor for decreased survival. J Pathol 2007;212:316–24.

12. Elayadi AN, Samli KN, Prudkin L, et al. A peptide selected by biopanning identifies the integrin $\alpha_v\beta_6$ as a prognostic biomarker for nonsmall cell lung cancer. Cancer Res 2007;67:5889–95.

13. Koopman Van Aarsen LA, Leone DR, Ho S, et al. Antibody mediated blockade of integrin $\alpha_v\beta_6$ inhibits tumor progression *in vivo* by a transforming growth factor-β-regulated mechanism. Cancer Res 2008;68:561–70.

14. McCarty JH. α_v Integrins lead the way for colorectal metastases. Clin Cancer Res 2008;14:6351–3.

15. Sheppard D, Rozzo C, Starr L, Quaranta V, Erle DJ, Pytela R. Complete amino acid sequence of a novel integrin β subunit (β_6) identified in epithelial cells using the polymerase chain reaction. J Biol Chem 1990;265:11502–7.

16. Breuss JM, Gallo J, Delisser HM, et al. Expression of the β6 integrin subunit in development, neoplasia and tissue-repair suggests a role in epithelial remodeling. J Cell Sci 1995;108:2241–51.

17. Breuss JM, Gillett N, Lu L, Sheppard D, Pytela R. Restricted distribution of integrin β6 messenger-RNA in primate epithelial tissues. J Histochem Cytochem 1993;41:1521–7.

18. Thomas GJ, Nystrom ML, Marshall JF. $\alpha_v\beta_6$ integrin in wound healing and cancer of the oral cavity. J Oral Pathol Med 2006;35:1–10.

19. Nemeth JA, Nakada MT, Trikha M, et al. α-v integrins as therapeutic targets in oncology. Cancer Invest 2007;25:632–46.

20. Sipos B, Hahn D, Carceller A, et al. Immunohistochemical screening for β_6-integrin subunit expression in adenocarcinomas using a novel monoclonal antibody reveals strong up-regulation in pancreatic ductal adenocarcinomas *in vivo* and *in vitro*. Histopathology 2004;45:226–36.

21. Zhang ZY, Xu KS, Wang JS, et al. Integrin $\alpha_v\beta_6$ acts as a prognostic indicator in gastric carcinoma. Clin Oncol 2008;20:61–6.

22. Hausner SH, DiCara D, Marik J, Marshall JF, Sutcliffe JL. Use of a peptide derived from foot-and-mouth disease virus for the noninvasive imaging of human cancer: generation and evaluation of 4-[^{18}F]fluorobenzoyl A20FMDV2 for *in vivo* imaging of integrin $\alpha_v\beta_6$ expression with positron emission tomography. Cancer Res 2007;67:7833–40.

23. Chen EL, Prinz RA. Long-term survival after pancreatic cancer treatment. Am J Surg 2007;194:S127–30.

24. Thomas GJ, Lewis MP, Hart IR, Marshall JF, Speight PM. $\alpha_v\beta_6$ integrin promotes invasion of squamous carcinoma cells through up-regulation of matrix metalloproteinase-9. Int J Cancer 2001;92:641–50.

25. Reilly RM, Kiarash R, Cameron RG, et al. ^{111}In-labeled EGF is selectively radiotoxic to human breast cancer cells overexpressing EGFR. J Nucl Med 2000;41:429–38.

26. Zasadny KR, Wahl RL. Standardized uptake values of normal tissues at PET with 2-[fluorine-18]-fluoro-2-deoxy-D-glucose - variations with body weight and a method for correction. Radiology 1993;189:847–50.

27. Ghannad F, Nica D, Fulle MIG, et al. Absence of $\alpha_v\beta_6$ integrin is linked to initiation and progression of periodontal disease. Am J Pathol 2008;172:1271–86.

28. Harris JM, Chess RB. Effect of PEGylation on pharmaceuticals. Nat Rev Drug Discov 2003;2:214–21.

29. Greenwald RB, Choe YH, McGuire J, Conover CD. Effective drug delivery by PEGylated drug conjugates. Adv Drug Deliv Rev 2003;55:217–50.

30. Sheppard D. Integrin-mediated activation of latent transforming growth factor β. Cancer Metastasis Rev 2005;24:395–402.

31. Duncan R. The dawning era of polymer therapeutics. Nat Rev Drug Discov 2003;2:347–60.

32. Liu S. Radiolabeled multimeric cyclic RGD peptides as integrin $\alpha_v\beta_3$ targeted radiotracers for tumor imaging. Mol Pharmaceuticals 2006;3:472–87.

33. Delbeke D, Pinson CW. Pancreatic tumors: role of imaging in the diagnosis, staging, and treatment. J Hepato Biliary Pancreatic Surg 2004;11:4–10.

34. Li CW, Heidt DG, Dalerba P, et al. Identification of pancreatic cancer stem cells. Cancer Res 2007;67:1030–7.

Cancer Research
The Journal of Cancer Research (1916–1930) | The American Journal of Cancer (1931–1940)

AACR American Association for Cancer Research

Targeted *In vivo* Imaging of Integrin α _vβ ₆ with an Improved Radiotracer and Its Relevance in a Pancreatic Tumor Model

Sven H. Hausner, Craig K. Abbey, Richard J. Bold, et al.

Cancer Res Published OnlineFirst June 23, 2009.